IOP Conference Series: Materials
Science and Engineering

PAPER • **OPEN ACCESS**

Mechanical Analysis of Sandwiched Maglev 2D-Positioning Stage

To cite this article: Ningran Song *et al* 2019 *IOP Conf. Ser.: Mater. Sci. Eng.* **677** 022030

IOP Conf. Series: Materials Science and Engineering **677** (2019) 022030 doi:10.1088/1757-899X/677/2/022030

Mechanical Analysis of Sandwiched Maglev 2D-Positioning Stage

Ningran Song[1], Guangxu Zhou[1, *], Mengmei Zhu[1], Shuyuan Ma[2], Yongyun Mu[1], Jia Gao[1]

[1]Institute of Automation, Shandong Academy of Sciences, Shandong Provincial Key Laboratory of Automotive Electronic Technology, Qilu University of Technology (Shandong Academy of Sciences) Jinan, China
[2]School of Mechanical Engineering Beijing Institute of Technology Beijing, China

*Corresponding author e-mail: zhouguangxu1124@163.com

Abstract. This paper proposes a two-dimensional magnetic positioning stage with a sandwiched coplanar structure. The novel symmetric compensation structure can realize the steady levitation of the platform, which is of vital importance to the positioning accuracy. To verify the reliability of the special structure, vibration modal, thermal deformation and mechanical deformation of the sandwiched maglev positioning stage under different working conditions are analyzed in finite element method. The simulation results show that this novel structure can meet the working requirements.

1. Introduction

With the development of traditional manufacture industry to nano manufacture industry, there exits urgent need for a large-stroke high-precision manufacturing platform to meet with the requirements of nano manufacturing, assembly, measurements and large-scale production. The magnetic levitation positioning stage rises in response, with the advantage of zero friction, no wear, no need of lubrication, long life, low power consumption, noiselessness and so on. Different kinds of maglev stages are designed, with or without rail support. To obtain multiple degrees of freedom, maglev stage with rail support [1-2] will own a redundant structure, which will affect the system response. Maglev stages without rail support [3-9] make use of the electromagnetic force to achieve levitation. This paper introduces a novel maglev stage with sandwiched structure [10], as shown in Fig. 1.

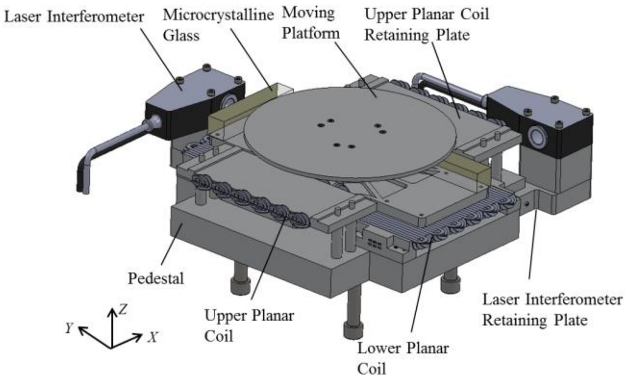

Figure 1. Schematic diagram of the sandwiched maglev stage.

The sandwiched maglev stage is composed of moving platform and pedestal. The moving platform is placed between the lower and upper planar coil, forming the sandwiched structure. Displacement in the horizontal direction is obtained by laser interferometer and microcrystalline glass. To increase the damping ratio of the whole system, an eddy current retarder is designed.

The sandwiched maglev stage needs high stiffness to satisfy the positioning accuracy, so mechanical analysis is necessary. Mechanical analysis includes static analysis and modal analysis. Static analysis studies the deformation of the stage under the working load. Modal analysis studies natural frequency and vibration modal of the stage under different working conditions. The finite element software ANSYS Workbench is used to do the mechanical analysis.

2. Structure of Sandwiched Maglev Stage

Moving platform is composed of working plate and mobile plate, as shown in Fig. 2. These two parts are coaxial mounted and connected by three flexible hinges. Four permanent magnet arrays are embedded on the upper and lower surfaces of the mobile plate. These mounted on the upper surface on *Y* axis are called the upper permanent magnet arrays, and the others mounted on the lower surface on *X* axis are called the lower permanent magnet arrays, which are the main electromagnetic units.

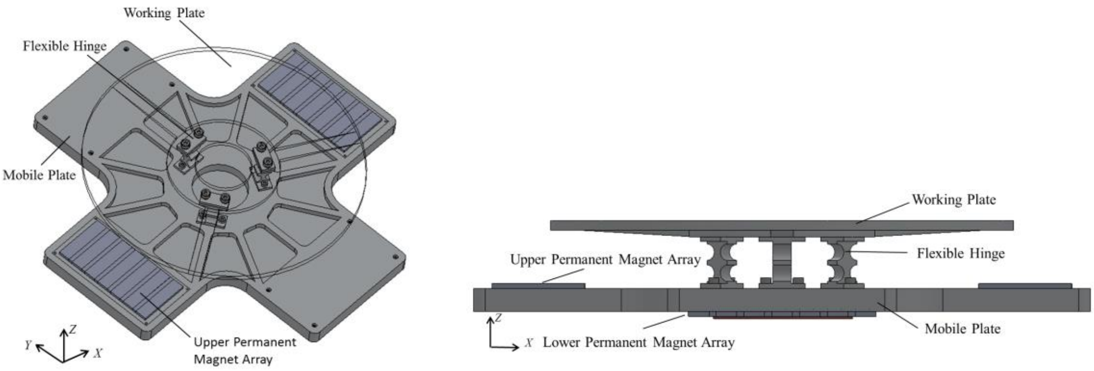

Figure 2. Structure of the moving platform.

To match up with the permanent magnet arrays, four planar coils are installed on the pedestal, as shown in Fig. 3. The upper planar coil works with the upper permanent magnet array, forming an attractive linear motor that can provide levitation force and driving force on *Y* axis. The lower planar coil works with the lower permanent magnet array, forming a repulsive linear motor that can provide levitation force and driving force on *X* axis. The eddy current retarder is also installed on the pedestal.

IOP Conf. Series: Materials Science and Engineering **677** (2019) 022030 doi:10.1088/1757-899X/677/2/022030

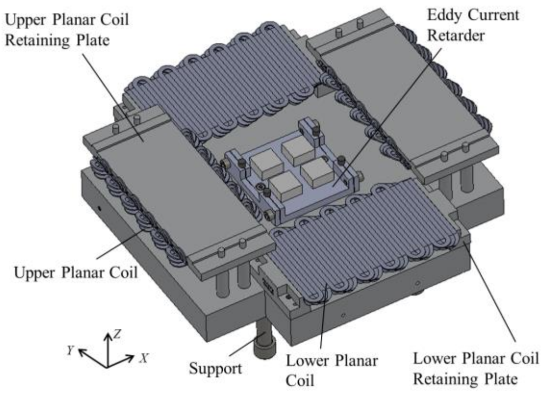

Figure 3. Structure of the pedestal.

The permanent magnet arrays are made of NdFeB, and the body of the maglev stage is made of aluminium alloy. Material properties are listed in Tab. 1.

Table 1. Material Property

Material	Material Property		
	Elasticity Modulus(Pa)	*Poisson's Ratio*	*Density*(kg/m^3)
Aluminium alloy	7.1×10^{10}	0.33	2770
NdFeB	1.6×10^{11}	0.24	7600

3. Electrothermal Analysis of Planar Coil

Planar coil is the main heating part in the sandwiched maglev stage. The thermal load condition when the coil is energized should be analyzed. Fig. 4 shows the initial condition added on the coil. End faces of three-phase winding are applied zero voltage to simulate the star connection. Three-phase current of $\theta = 0^\circ, \phi = 0^\circ, I = 6A$ (working current) are applied on the three head faces. The temperature condition is chosen as heat convection, and the heat transfer coefficient is 25. Set the initial condition to room temperature as $22^\circ\mathrm{C}$.

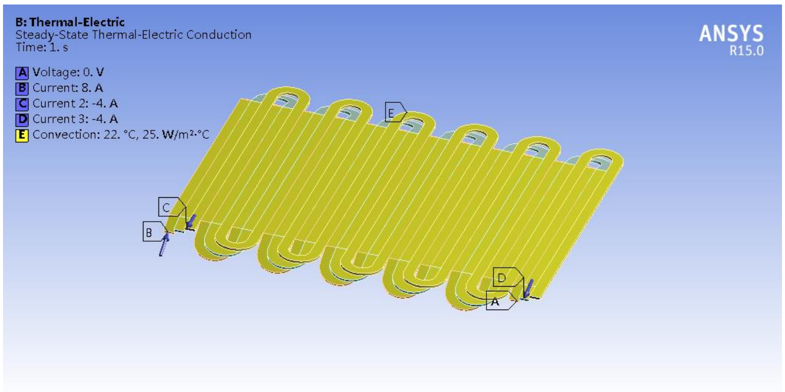

Figure 4. The finite element model of planar coil.

Fig. 5 shows the temperature distribution of the planar coil. The bulk temperature of the planar coil is close to the room temperature, only tiny changes on the head faces. As the effect of the tiny changes on the whole magnetic levitation system can be negligible, the following of the paper won't analyze the temperature effect.

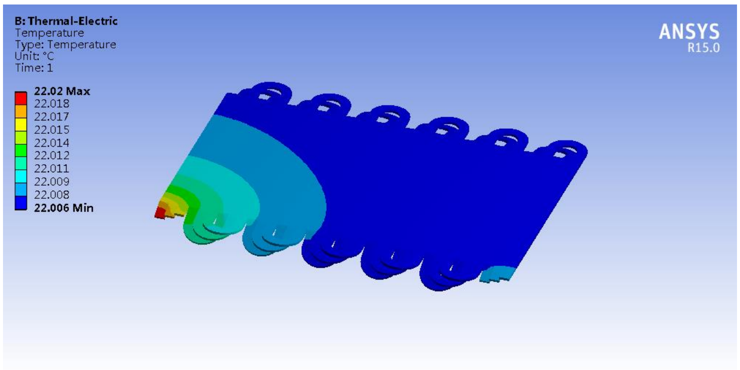

Figure 5. Temperature distribution of the planar coil.

4. Static Analysis of the Moving Platform

Since the moving platform and the pedestal are separated relatively, they will be analyzed separately in this paper.

4.1. Mechanical Deformation

The moving platform is affected by gravity and electromagnetic force when suspended, which will cause bending deformation. If the deformation is beyond the allowable values, the accuracy of suspension and positioning can't be guaranteed, which are mainly relied on the permanent magnet arrays. The deformation of the working plate should also be focused to avoid negative influence to the workpiece placed there. Fig. 6(a) is the finite element model of the moving platform. The Lorentz forces on the positive *Z* direction are applied on the working faces of upper and lower permanent magnet arrays as pressure, which are shown in Fig. 6(b). There is no constraint when suspended.

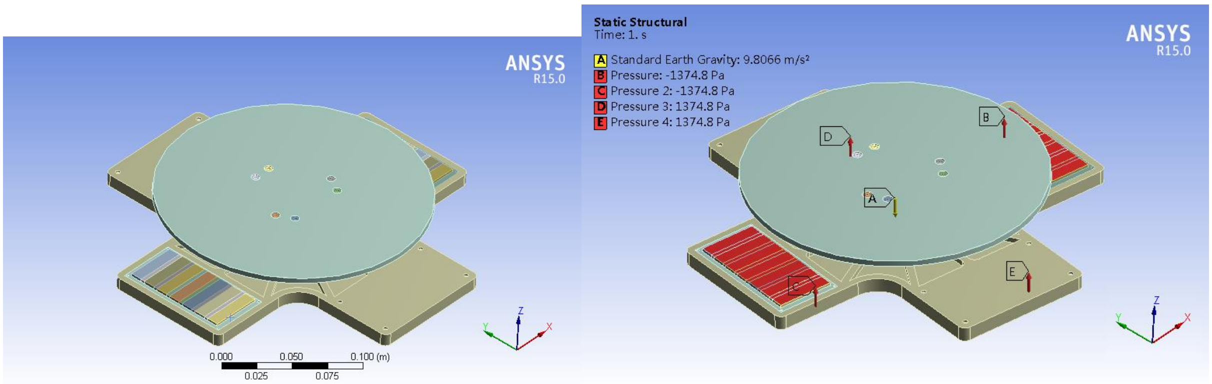

(a) Finite element model (b) Force diagram

Figure 6. Finite element model and force diagram of the moving platform.

The upper permanent arrays fixed on the mobile plate meet with the requirement of suspension and positioning on *Y* axis, so deformation on these two directions are focused, as shown in Fig. 7. The maximum deformation on *Z* axis is 1.6255 μm, which is allowable compared to the levitation height of 500 μm. The maximum deformation on *Y* axis is 0.0685 μm and is symmetrical.

IOP Conf. Series: Materials Science and Engineering **677** (2019) 022030 doi:10.1088/1757-899X/677/2/022030

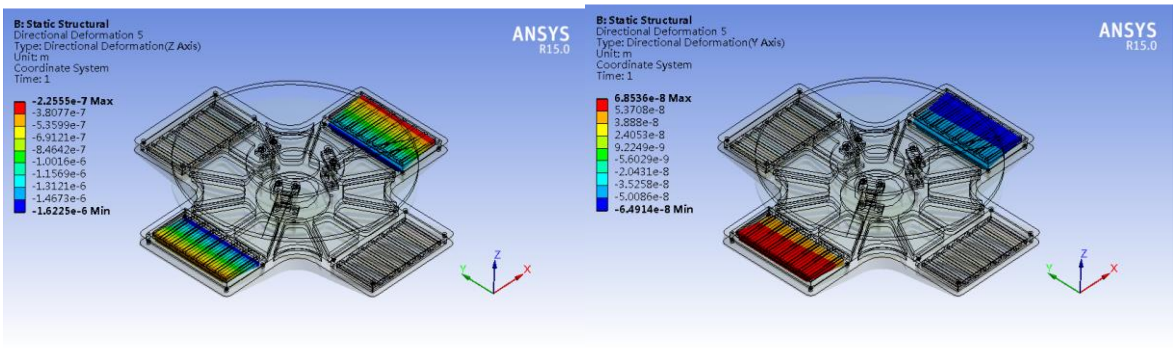

(a) Deformation on Z axis (b) Deformation on Y axis

Figure 7. Deformation of the upper permanent magnet arrays.

The lower permanent magnet arrays fixed on the mobile plate meet with the requirement of suspension and positioning on X axis, so deformation on these two directions are concerned, as shown in Fig. 8. The maximum deformation on Z axis is 1.6319 μm, and the maximum deformation on X axis is 0.0704 μm, which are similar to the upper ones.

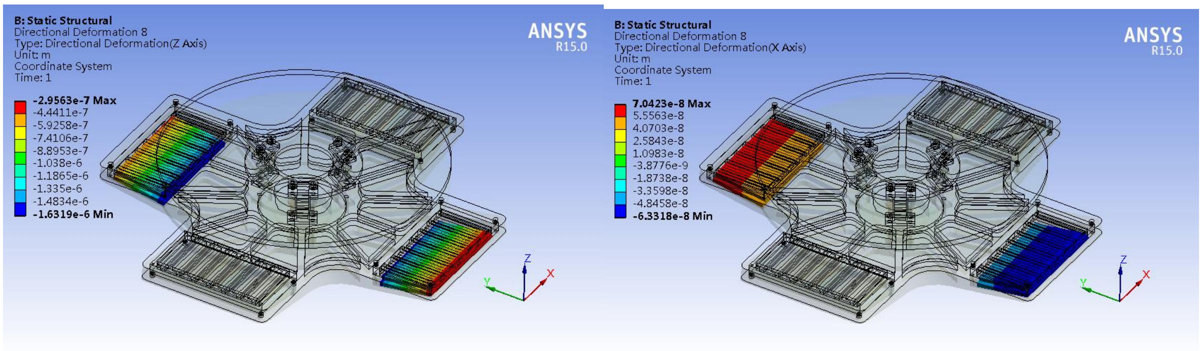

(a) Deformation on Z axis (b) Deformation on X axis

Figure 8. Deformation of the lower permanent magnet arrays.

4.2. Vibration Modal

The moving platform is unrestricted when suspended, so the former six orders are rigid body modes. The 7th to 12th natural frequency are listed in Tab. 2, and the corresponding modal shapes are shown in Fig. 9. The 7th modal shape is the vibration of the permanent magnet arrays on Z axis. The 8th modal shape is the vibration of the moving platform on Z axis. The 9th natural frequency is similar to the 10th, the corresponding modal shape is the rotation about Y axis and X axis respectively. The modal shape of 11th and 12th is the twisting of the moving platform.

Table 2. Natural Frequency of the Moving Platform

Order	*Frequency*(Hz)
7	254
8	423
9	479
10	486
11	619
12	782

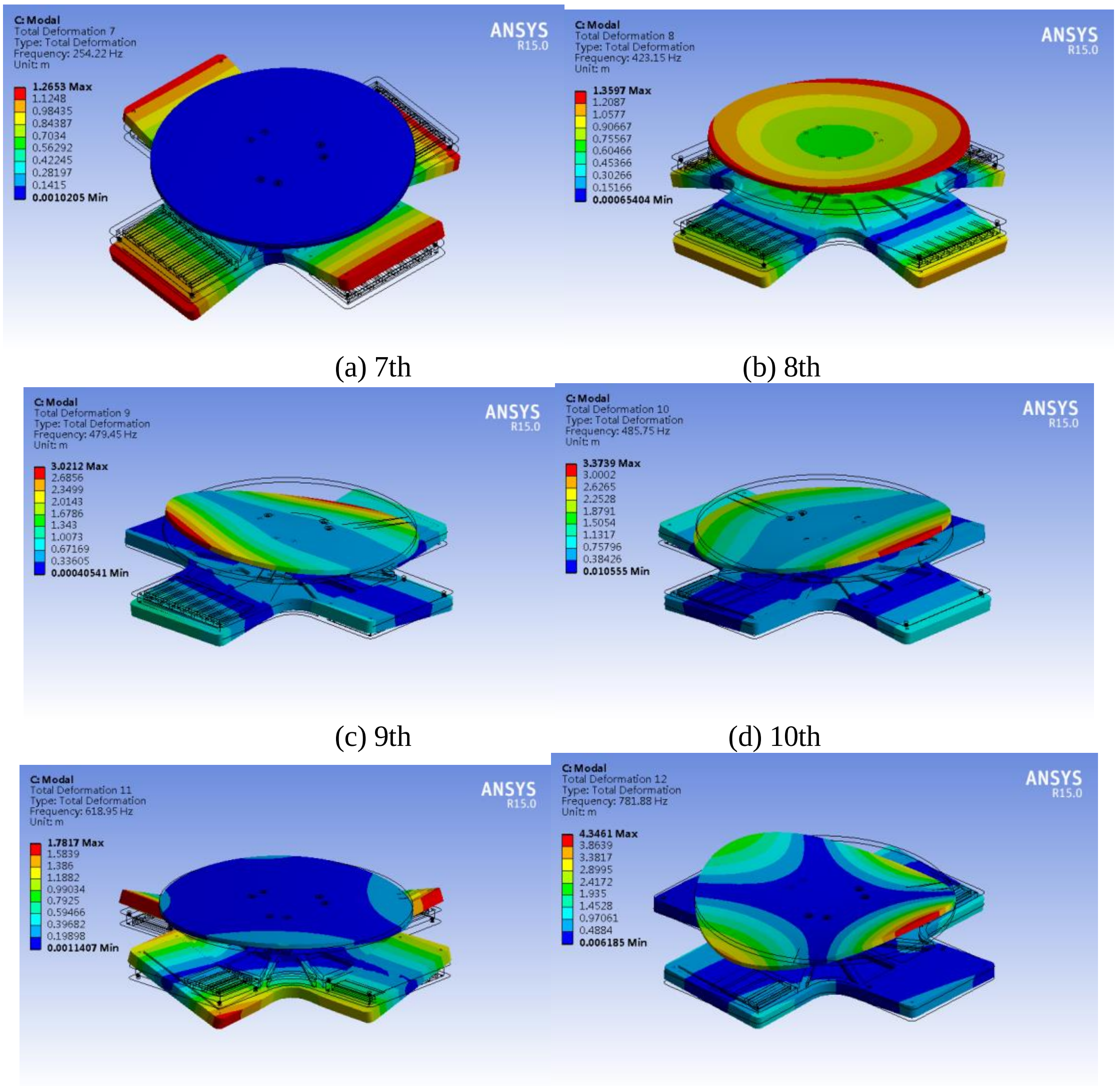

(a) 7th (b) 8th

(c) 9th (d) 10th

(e) 11th (f) 12th

Figure 9. Each order modal shape of the moving platform.

As shown in the analysis results, the weak areas are mainly the permanent magnet arrays and the mobile plate. The impact of the working plate is mitigated due to the symmetrical structure and the flexible hinge.

5. Static Analysis of the Pedestal

To the pedestal, forces and deformation are focused on the planar coil retaining plates, where should be concerned. The deformation of laser interferometer retaining plates should also be concerned since it is related to the feedback of positioning directly. The eddy current retarder is removed here.

5.1. Mechanical Deformation

Fig. 10(a) shows the finite element model of the pedestal. To guarantee positioning of the moving platform, planar coil is designed wider and longer than the permanent magnet array. According to Newton’s third law, planar coil burdens electromagnetic force whose numerical value equal to moving platform’s gravity. Stress surfaces are made on the planar coil retaining plate, with permanent magnet array’s length and planar coil retaining plate’s width. As shown in Fig. 10(b), red faces D and E, are stress surfaces of the planar coil retaining plate on *X* axis. Stress surfaces of the planar coil retaining plate on *Y* axis are on the bottom face, labeled as face B and C. The electromagnetic forces are applied on the stress faces of upper and lower permanent magnet arrays as pressure. The four supports are fully constrained.

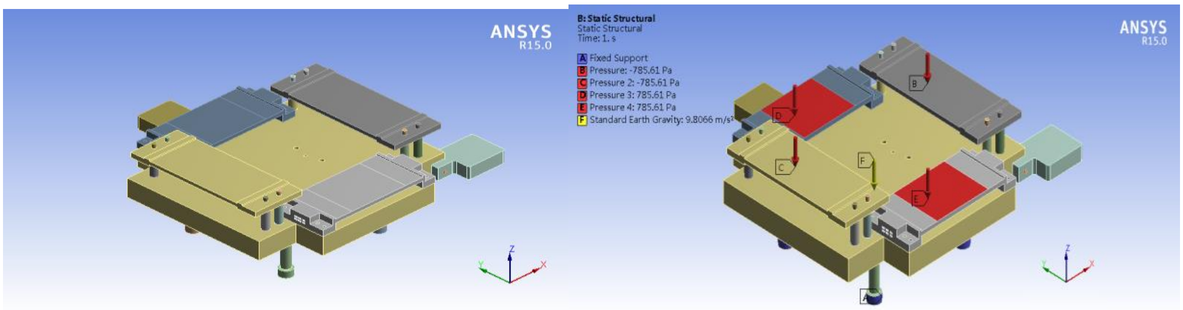

(a) Finite element model (b) Force diagram

Figure 10. Finite element model and force diagram of the pedestal.

The upper planar coil cooperates with the upper permanent magnet array to realize levitation and positioning on *Y* axis. Fig. 11 shows the deformation of upper planar coil retaining plate on *Z* axis and *Y* axis. The maximum deformation on *Z* axis is 1.4311 μm, which is allowable compared to the levitation height of 500 μm. The maximum deformation on *Y* axis is 0.0887 μm and is symmetrical.

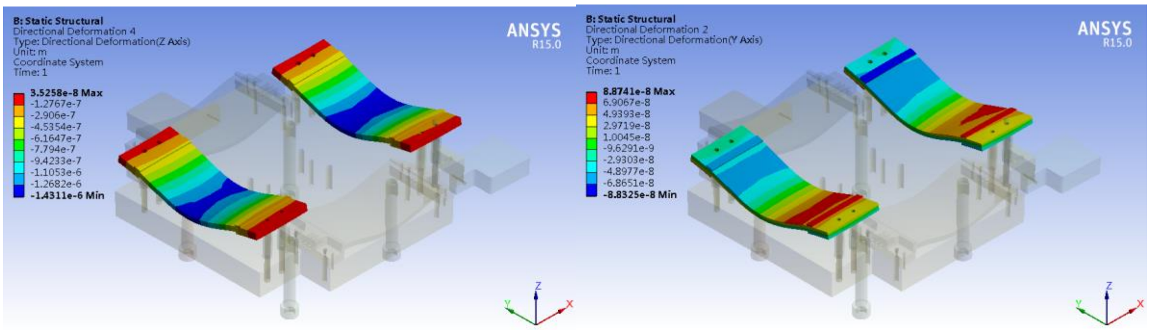

(a) Deformation on *Z* axis (b) Deformation on *Y* axis

Figure 11. Deformation of the upper planar coil retaining plate.

The lower planar coil cooperates with the lower permanent magnet array to realize levitation and positioning on *X* axis. Fig. 12 shows the deformation of lower planar coil retaining plate on *Z* axis and *X* axis. The maximum deformation on *Z* axis is 0.8469 μm, and the maximum deformation on *X* axis is 0.0582 μm. The lower planar coil retaining plate is not elevated as the upper one, so its maximum deformation on *Z* axis is smaller.

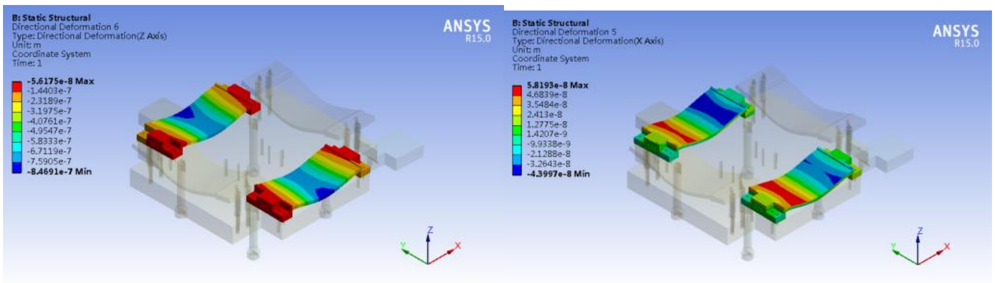

(a) Deformation on *Z* axis (b) Deformation on *X* axis

Figure 12. Deformation of the lower planar coil retaining plate.

Due to the instruction of laser interferometer, the installation error should be controlled within 8 μm. Fig. 13 shows the deformation of laser interferometer retaining plate on *X* axis. The maximum total deformation is 0.2828 μm, and the maximum deformation on *X* axis is 0.0057 μm, which meet with the requirements.

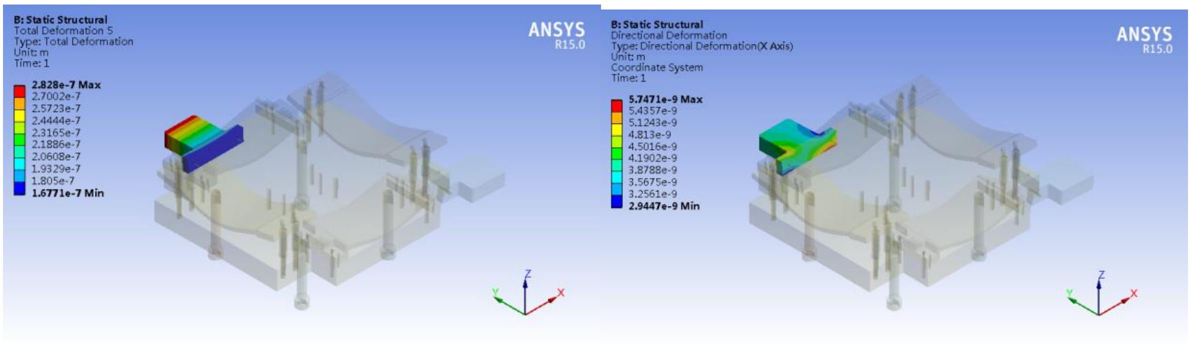

(a) Total deformation (b) Deformation on *X* axis

Figure 13. Deformation of the laser interferometer retaining plate on *X* axis.

Fig. 14 shows the deformation of laser interferometer retaining plate on *Y* axis. The maximum total deformation is 0.3612 μm, and the maximum deformation on *Y* axis is 0.0238 μm, which meet with the requirements.

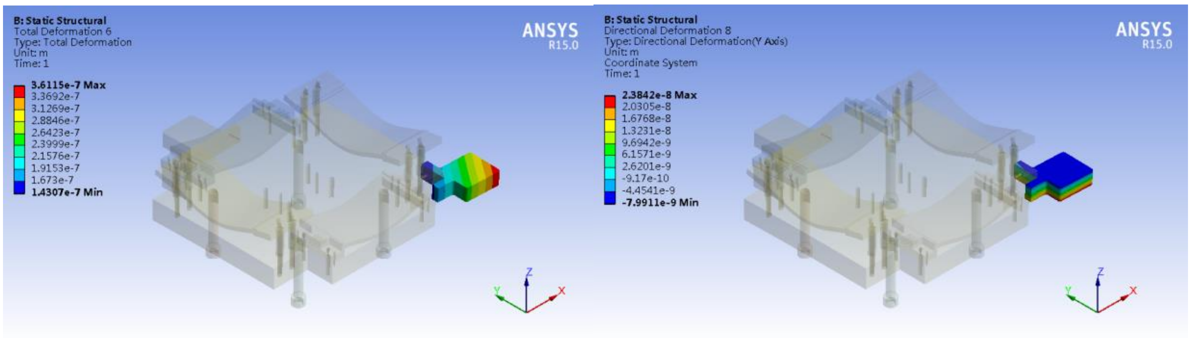

(a) Total deformation (b) Deformation on *Y* axis

Figure 14. Deformation of the laser interferometer retaining plate on *Y* axis.

To verify the stability of the pedestal when the moving platform moves to extreme position, stress surfaces at different position are made, as shown in Fig. 15 and Fig. 16. Fig. 15 simulates the condition when the moving platform moves to the edge of *X* axis on negative direction and the edge of *Y* axis on positive direction. It is called working condition 2. And the condition where the moving platform stays at the middle is called working condition 1. Fig. 16 simulates the condition when the moving platform moves to the edge of *X* axis on positive direction and the edge of *Y* axis on negative direction, called working condition 3.

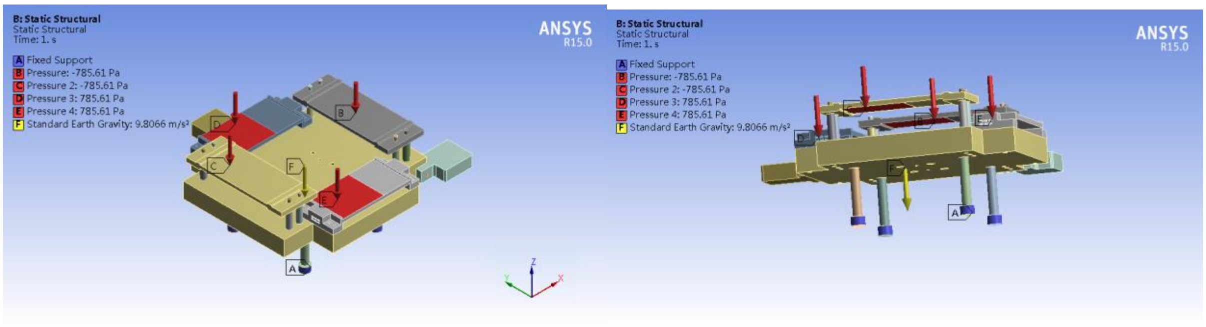

Figure 15. Force diagram of the pedestal under working condition 2.

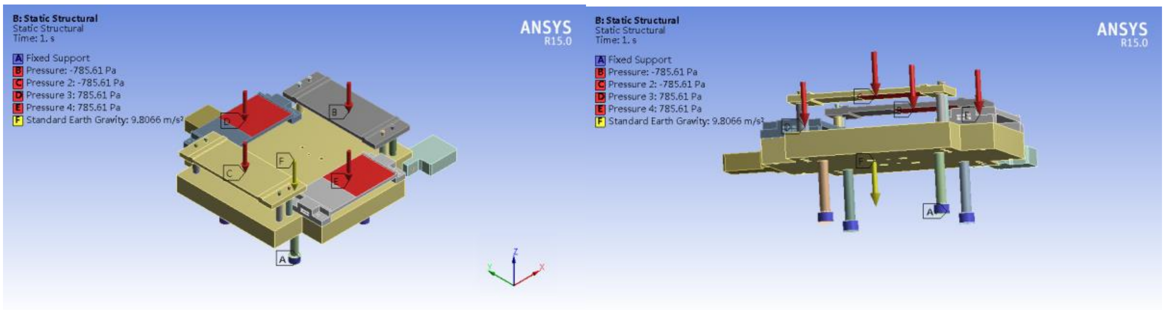

Figure 16. Force diagram of the pedestal under working condition 3.

Maximum deformations of the upper and lower planar coil retaining plate, laser interferometer retaining plate on *X* axis and *Y* axis are listed in Tab. 3. It shows that maximum deformations of the main parts of the pedestal are similar under three working conditions. And maximum deformations of the laser interferometer retaining plate on *X* axis and *Y* axis under three working conditions are all smaller than 8 μm, which satisfy the installation requirements.

Table 3. Maximum Deformation of the Main Part of the Pedestal under Different Working Conditions

Part	Maximum Deformation (μm)			
		Working condition 1	*Working condition 2*	*Working condition 3*
Upper planar coil retaining plate	*Z*	1.4311	1.3418	1.3031
	Y	0.0887	0.1621	0.1584
Lower planar coil retaining plate	*Z*	0.8469	0.7329	0.7279
	X	0.0582	0.0528	0.0447
Laser interferometer retaining plate on *X* axis	Total	0.2828	0.2896	0.2766
	X	0.0057	0.0060	0.0068
Laser interferometer retaining plate on *Y* axis	Total	0.3612	0.3409	0.3805
	Y	0.0238	0.0241	0.0227

5.2. Vibration Modal
Natural frequencies of the pedestal under three working conditions are listed in Tab. 4. Values are similar, which indicate the stability of the system.

Table 4. Natural Frequency of the Pedestal

Order	Frequency(Hz)		
	Working Condition 1	*Working Condition 2*	*Working Condition 3*
1	289	289	288
2	324	324	323
3	325	325	324
4	1065	1054	1070
5	1112	1010	1106
6	1181	1176	1194

Since the modal shapes of three working conditions are similar, here take the modal shape of working condition 1 as example to describe in detail, as shown in Fig. 17. The 1th modal shape is the twisting of four supports. Natural frequencies of 2nd and 3rd are similar, so are the modal shape, which are the swing of four supports. The modal shape of 4th and 5th is deformation of the upper planar coil retaining plates and laser interferometer retaining plate on *Y* axis. The modal shape of 6th is deformation of the laser interferometer retaining plate on *Y* axis, lower and upper planar coil retaining plates.

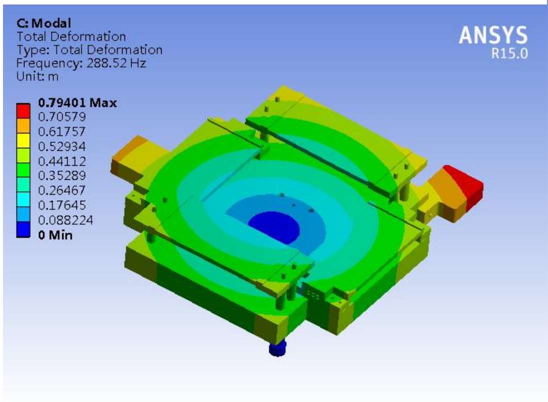

(a)1st

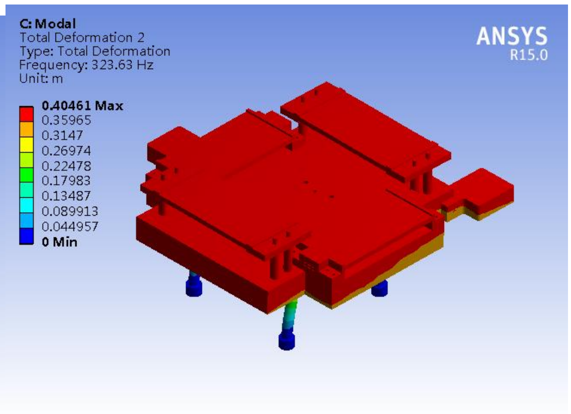

(b)2nd

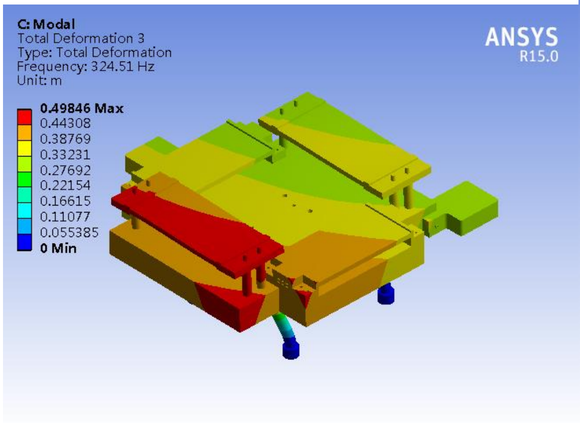

(c)3rd

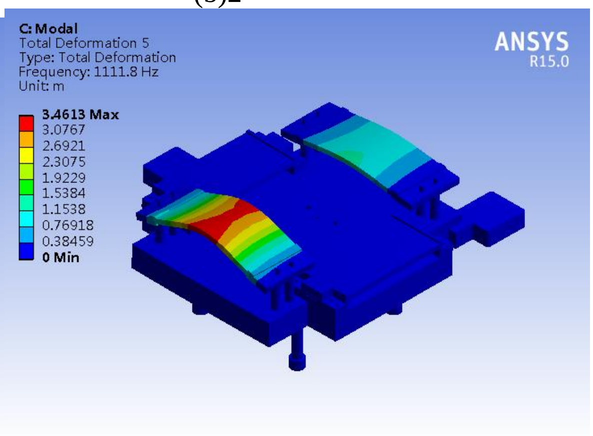

(d) 4th

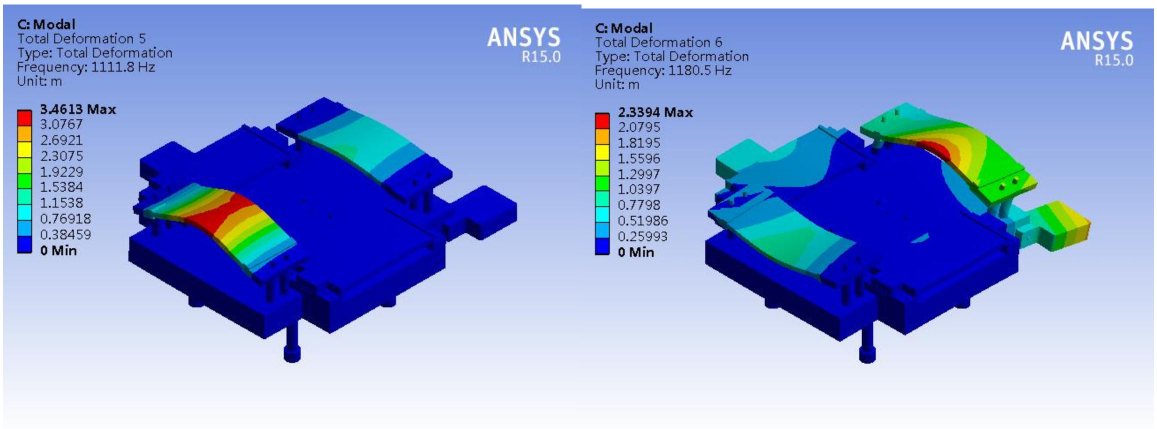

(e)5th (f)6th

Figure 17. Each order modal shape of the pedestal.

As shown in the analysis results, the weak areas are mainly the four supports and the upper planar coil retaining plates. The supports can be reinforced. Planar coil retaining plates in different height are the key to sandwiched structure maglev platform, which will bring more advantages compared with the possible deformation effects.

6. Conclusion

To ensure reliability of sandwiched maglev stage from the view of mechanical structure, static analysis of the moving platform and pedestal under different working conditions are done. Mechanical deformation and vibration modal of main parts are analyzed. The results show that the sandwiched structure maglev stage is reliable enough to meet with the job requirements, which lay a good foundation for subsequent research.

Acknowledgments

This work was supported by the Natural Science Foundation of Shandong Province (Grant No. ZR2019BEE038), Natural Science Foundation of Shandong Province (Grant No. ZR2019MEE103), National Natural Science Foundation of China (Grant No. 51375052).

References

[1] Duan Jian, Guo Ningping, Zhou Haibo, “Thermal analysis of novel linear maglev transportation platform,” Proceedings of the CSEE, vol. 31, 2011, pp. 114-120, 2011.
[2] Jing Minqing, Liu Heng, Liang Jinxing, “Two dimensional high precision positioning maglev stage,”Journal of XiAn Jiaotong University, vol. 42, 2008, pp.1377-1381.
[3] David L. Trumper, Sean M. Olson, “Linearizing Control of Magnetic Suspension Systems,” IEEE Transactions on Control Systems Technology, vol. 5, 1997, pp. 427-438.
[4] Takeshi Kurihara, Takayoshi Narita, “Effect of a Magnetic Field from the Horizontal Direction on a Magnetically Levitated Steel Plate(Fundamental Consideration on the Levitation Performance),” International Journal of Applied Electromagnetics and Mechanics, 2016, doi10.3233/JAE-162144.
[5] Won-jong Kim, “Six-axis Nano-positioning with Planar Magnetic Levitation,” IEEE-NANO, vol. 3, 2001, pp. 174-179.
[6] Shih-Kang Kuo, Ximin Shan, Chia-Hsiang Menq, “Large Travel Ultra Precision x-y-θ Motion Control of a Magnetic-suspension Stage,” IEEE/ASME Transactions on Mechatronics, vol. 8, 2003, pp. 334-341.
[7] Takahisa Ohji, Fuyuki Kato, A Comparative Numerical Study of Repulsive Forces for Stabilizing a Rectangular Aluminum Plate between AC Induction Type and AC Ampere

Type Magnetic Levitation Methods, International Journal of Applied Electromagnetics and Mechanics, vol. 45, 2014, pp. 895-901.

[8] Shalom Dovber Ruben, Modeling, Control, and Real-time Optimization for a Nano-precision System, University of California, 2010.

[9] Xiaoguang Wang, Xiao Zhang, Modeling of an Incomplete Constraint Magnetic Levitation System, International Journal of Applied Electromagnetics and Mechanics, vol. 49, 2015, pp. 363-373.

[10] Ningran Song, Shuyan Ma, Zongqing Zhang, A numerical study of forces for sandwiched maglev stage, International Journal of Appled Electromagnetics and Mechanics, vol. 55, 2017, pp. 89-100.